Expression of target optical properties in subsurface polarization-gated imaging

Ralph Nothdurft and Gang Yao

Department of Biological Engineering, University of Missouri-Columbia, Columbia, MO 65211
renothdurft@mizzou.edu, yaog@missouri.edu

Abstract: We examined the expression of target optical properties in subsurface polarization imaging under linearly and circularly polarized illumination. Reflecting, scattering, and absorption targets were imaged in tissue mimic phantoms. The polarization gated images were compared with raw and unpolarized images to determine image enhancement as a function of target depth. The experimental results were also compared with Monte-Carlo simulations to study the model's applicability. Our results indicated that polarization imaging provided a means to separate different optical targets where they would otherwise appear similar under unpolarized light.

OCIS codes: (260.5430) Polarization (170.3880) Medical and Biological Imaging (290.4020) Multiple scattering (290.7050) Turbid media

References and links

1. S. G. Demos and R.R. Alfano, "Optical polarization imaging," Appl. Opt. **36**, 150-155 (1997).
2. W. Groner, J. W. Winkelman, A. G. Harris, C. Ince, G. J. Bouma, K. Messmer, and R. G. Nadeau, "Orthogonal polarization spectral imaging: A new method for study of the microcirculation," Nature Medicine **5**, 1209-1213(1999).
3. S. G. Demos, H. B. Radousky, and R. R. Alfano, "Deep subsurface imaging in tissues using spectral and polarization filtering," Opt. Express **7**, 23-28(2000).
4. S. P. Morgan and I.M. Stockford, "Surface-reflection elimination in polarization imaging of superficial tissue," Opt. Lett. **28**, 114-116(2003).
5. V. Backman, R. Gurjar, K. Badizadegan, I. Itzkan, P.R. Dasari, L.T. Perelman, and M.S. Feld, "Polarized light scattering spectroscopy for quantitative measurement of epithelial cellular structures in situ," IEEE J. Quantum Electron **5,** 1019-1026(1999)
6. S. G. Demos, A.J. Papadopoulos, H. Savage, A.S. Heerdt, S. Schantz, and P.R. Alfano, "Polarization filter for biomedical tissue optical imaging," Photochemistry & Photobiology **66**, 821-5(1997).
7. S. L. Jacques, J. R. Roman, and K. Lee, "Imaging superficial tissues with polarized light," Lasers in Surg. & Med. **26**, 119–129(2000).
8. S. L. Jacques, J. C. Ramella-Roman, and K. Lee, "Imaging skin pathology with polarized light," J. Biomed. Opt. **7**, 329-340(2002).
9. V. Sankaran, M.J. Everett, D.J. Maitland, and J.T.Walsh, "Comparison of polarized-light propagation in biological tissue and phantoms," Opt. Lett. **24**, 1044-1046(1999).
10. V. Sankaran, J. T. Walsh, and D. J. Maitland, "Polarized light propagation through tissue phantoms containing densely packed scatterers," Opt. Lett. **25,** 239-241(2000).
11. V. Sankaran, J. T. Walsh, and D. J. Maitland, "Comparative study of polarized light propagation in biologic tissues," J. Biomed. Opt. **7**, 300-306(2002).
12. X. Ni and R. R. Alfano, "Time-resolved backscattering of circularly and linearly polarized light in a turbid medium," Opt. Express **29**, 2773-2775(2004).
13. G. Yao, "Differential optical polarization imaging in turbid media with different embedded objects," Opt. Comm. **241**, 255-261(2004).
14. Y. Pan, R. Birngruber, R. Engelhardt, "Contrast limits of coherence-gated imaging in scattering media," Appl. Opt. **36**, 2979-2983 (1997).
15. A. D. Kim and M. Moscoso, "Backscattering of circularly polarized pulses," Opt. Lett. **27**, 1589–1591 (2002).
16. I. M. Stockford, S. P. Morgan, P. C. Y. Chang, and J. G. Walker, "Analysis of the spatial distribution of polarized light backscattered from layered scattering media," J. Biomed. Opt. **7**, 313-320(2002)
17. H. J. van Staveren, C. J. M. Moes, J. van Marle, S. A. Prahl, and M. J. C. van Gemert, "Light scattering in Intralipid-10% in the wavelength range of 400-1100nm," Appl. Opt. **30**, 4507-4514(1991).
18. N. Ghosh, H. S. Patel, and P. K. Gupta, "Depolarization of light in tissue phantoms – effect of a distribution in the size of scatterers," Opt. Express **11**, 2198-2205(2003).

#6729 - $15.00 US Received 28 February 2005; revised 19 May 2005; accepted 19 May 2005

1. Introduction

Tissue optical properties are indicative of composition. Discerning the optical properties of a target involves untangling the photon-media and photon-target interaction. This is initially a question of detection: whether light from the target area appears differently from the background. It is next a question of diagnosis: whether the difference in reflected light can be attributed to specific properties of the target.

Subsurface polarization imaging is a direct extension of common video-imaging setup by incorporating optical elements to choose illumination polarization states and detect specific polarized backscattering light [1]. So far, most of the relevant studies have focused on using polarization gating to reject surface glare for probing deep tissue [2-4], or to selectively detect photons from superficial layers [5]. On the other hand, using polarization responses as contrast mechanisms has not been well studied in the context of imaging. Demos et al. [6] reported that bulk cancerous tissues had higher depolarization ratio than normal tissues. Jacques et al. [7, 8] further demonstrated that polarization-sensitive detection could indeed discriminate different skin pathological features. However the detailed mechanisms behind these phenomena are not quite clear in inhomogeneous samples. In addition, linearly polarized light is usually used because they're easy to calibrate and handle, while there were studies indicating circularly polarized light propagated differently inside scattering media [9-12]. Therefore, different polarized light could be utilized to fully reveal the optical properties difference.

A thorough understanding of the contrast mechanisms involved in polarization imaging is essential for biomedical applications. Based on previous studies, it has been established that diseased tissues have different optical properties than normal tissues. Such differences may manifest themselves in the polarization images and be used as a basis for medical diagnosis. A recent Monte-Carlo study [13] showed that different types of objects appeared differently in polarization images, which implied that polarization detection could be used to identify different optical targets. In this paper, a series of studies were performed in tissue simulating phantoms to investigate the expression of target optical properties in subsurface polarization imaging. Three types of targets were studied: reflecting, scattering, and absorption, which represent different tissues compositions and potential contrast mechanisms in imaging. Two polarization processing methods were examined in the study: the differential polarization imaging and the degree of polarization imaging.

2. Materials and methods

The tissue mimic phantom consisted of *Intralipid* (Intralipid™ 20%, Kabi Pharmacia, Clayton, NC) and Indian ink diluted in distilled water. *Intralipid* solution has been widely used to make tissue mimic phantom. Various *Intralipid* and ink concentrations were used to make samples with scattering coefficients μ_s = 15−60cm^{-1}, anisotropy g=0.83, and absorption coefficient μ_a = 0.05−0.2 cm^{-1}. Three types of 3×3mm^2 targets were embedded in the scattering phantom. They represented three distinct contrast mechanisms: reflecting, scattering, and absorption. The reflecting target was a microscope cover slip sputter-coated with a 120nm layer of platinum. The other targets were plastic backing coated with a thick layer of model paint. Black paint and white paint served as our highly absorbing and highly scattering targets respectively. Glossy and flat versions of both colors were tested to examine the impact of fine surface features.

Targets were mounted on a wire arm attached to a vertical stage. The wire arm was designed so that only a very small area directly beneath the target was obstructed. The vertical stage allowed continuous height adjustments with 0.01mm resolution. The depth of material below the target was significantly greater than the target depths examined so that the phantoms can be treated as semi-infinite media. A Monte-Carlo simulation program [13] was also used to examine the impact of target properties. Simulation parameters were set to those used in the experiments.

#6729 - $15.00 US Received 28 February 2005; revised 19 May 2005; accepted 19 May 2005

2.1 Image acquisition

Figure 1 shows a diagram of the experimental setup. A He-Ne laser provided 10mW of polarized light at 633nm wavelength. The laser beam size was expanded to illuminate a 20mm sample area at 45° incidence. A variable waveplate (VW) selected either linearly or circularly polarized light, and allowed fine-tuning of circular polarized light to compensate for other components in the system. Light returning from the phantom was captured at normal incidence after passing through a quarter waveplate (QW) and a linear polarizer (P). A CCD camera (Pulnix TM-7AS) captured 640x480 8bit gray scale images. The camera aperture accepted photons within 1.7° over a 16mm by 12mm imaging area. The focal depth was sufficient to cover the full range of heights measured. The polarization precision was carefully calibrated. When the polarizers were finely adjusted with a power meter in place of the camera and a mirror in place of the phantom, polarization extinction ratios of 0.11‰ and 0.14‰ were achieved for linearly and circularly polarized light, respectively.

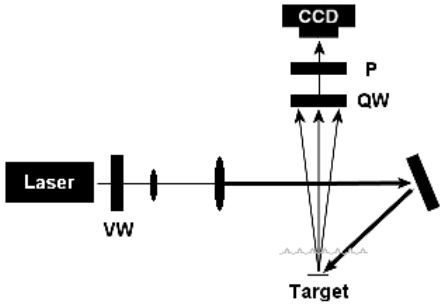

Fig. 1. Schematic diagram of experimental setup.

The resulting images were acquired into a computer for recording. Multiple averaging was performed at the time of capture to reduce speckle noise. In order to compensate for the inhomogeneity in the incident light, an image was taken for each set with no target present. This base image was smoothed with a Gaussian kernel and used to normalize the other images in the set. The normalization was applied to the raw images prior to analysis.

2.2 Image processing and contrast

The four raw component images consisted of the linearly and circularly co-polarized (CO) and cross-polarized (CR) images post-normalization. The pixel values for the components were straightforward representation of illumination ranging from 0 to 255. When CO and CR components are combined we get the equivalent of an unpolarized image, and here too the values represent illumination. Two different processing methods were evaluated in the experiments: differential polarization (DIFF) image, and degree of polarization (POL) image. The DIFF image was calculated as:

$$DIFF = CO - CR \tag{1}$$

The corresponding pixel values were from -255 to 255. The POL image was calculated as:

$$POL = \frac{DIFF}{(CO + CR)} \tag{2}$$

The corresponding pixel values were from -1 to 1. To make full use of the range of data available we did not take the absolute value of these two combinations. The DIFF image represented the extent to which CO is greater than CR, while the POL represented the degree of *co-polarization*, both of which can be negative.

For image display, the local palette of each image was rescaled to the full 8-bit range available without further processing. All images shown corresponded to areas of $12\times12mm^2$. When interpreting the images, it is important to keep in mind that image appearance depends

#6729 - $15.00 US Received 28 February 2005; revised 19 May 2005; accepted 19 May 2005

on the relative pixel values between target and background. For example, a dark target in a POL image means that the amount of light had a lower co-polarization than the background.

For a quantitative comparison, we calculated the visibility of the target against the background with:

$$contrast = \left| \frac{I_{obj} - I_{bg}}{I_{obj} + I_{bg}} \right| \tag{3}$$

where I_{obj} was calculated by averaging the middle quarter of the object, and I_{bg} was calculated by averaging pixels far away from the object. Contrast was capped at 1 if target and background values were of different signs with the justification that the difference in sign made the target trivial to detect. A mismatch of sign only occurred for DIFF and POL images when the target CR was higher than CO. For example, this occurred when circular polarization undergoes reversed helicity because of reflection. The depths of the objects were calculated in mean-free-path (*mfp*) units, which were defined as the inverse of the summation of the absorption coefficient μ_a and the scattering coefficient μ_s.

Each measurement was performed three times and the calculated contrast values were averaged. The contrast faithfully represented the target visibility with one caveat: because of the subtraction involved in their calculation, the DIFF and POL images had a lower signal to noise ratio. This can cause an apparent mismatch between the contrast value and the image. We evaluated the noise level at the target location by computing the relative pixel standard deviation (standard deviation / average pixel value). In the component and unpolarized image the noise level was roughly 1%, while in the DIFF and POL it was ~7.5%. This level did not necessarily indicate a visible limit, but beyond this point the image quality dropped off dramatically.

3. Results

3.1 Reflecting target

Reflection as a contrast mechanism can originate from the layer boundaries of a multilayer tissue structure. A reflecting target has also been used previously as a model to study the penetration depth of coherent imaging system [14]. For a subsurface imaging system, a reflecting target essentially folds the light space. For circular polarization the result is reversed helicity. Figure 2 shows a set of images of an embedded high reflective object. The background medium had a scattering coefficient of $30cm^{-1}$, and absorption coefficient of $0.1cm^{-1}$.

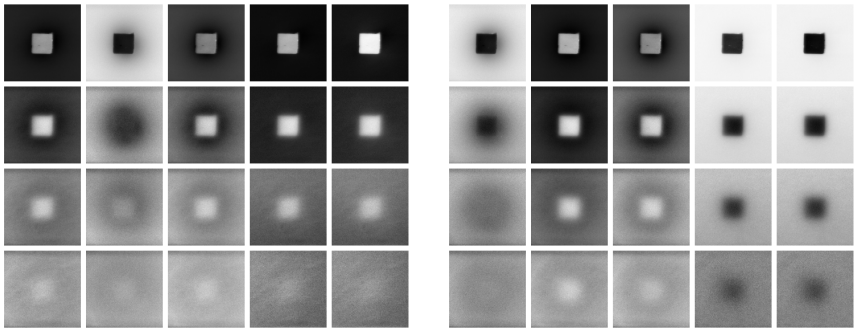

(a) (b)

Fig. 2. Image results of a reflecting target acquired with (a) linearly and (b) circularly polarized light. CO, CR, Unpolarized, DIFF, and POL images are listed from left column to right column. Rows correspond to target depth at 1.5, 4.5, 7.5, and 10.5mfp.

The target region in the raw images was composed primarily from photons from the target.

#6729 - $15.00 US Received 28 February 2005; revised 19 May 2005; accepted 19 May 2005

For shallow depths the result was a very bright target in linear CO and a dark target for linear CR. The reversed helicity resulted in a dark CO and bright CR targets under circular polarization. For highly scattering phantoms, those dark targets went through a crossover point where both the CO and CR images had targets brighter than the background because of the increased multiple scattering. The bright target in the linear POL indicated higher co-polarization than the background, while the dark target in circular POL indicated higher cross-polarization caused by reflection.

Figure 3 shows the detailed contrast behavior at different object depths. For linearly polarized light, CO images had better contrast than CR images. Linear DIFF and POL offered significant contrast improvement with DIFF being just slightly better. For circularly polarized light, the CR component gave better contrast than CO. The circular DIFF and POL contrast were identical and offer significantly improved contrast. Circular polarization led to a much higher contrast in the DIFF/POL images with a small increase in maximum visible depth. Both linear and circular raw images (CO and CR) had similar imaging depths as their gated combinations. Although DIFF and POL contrast have different physical interpretations, they overlapped completely under circularly polarized illumination and closely matched with linearly polarized light.

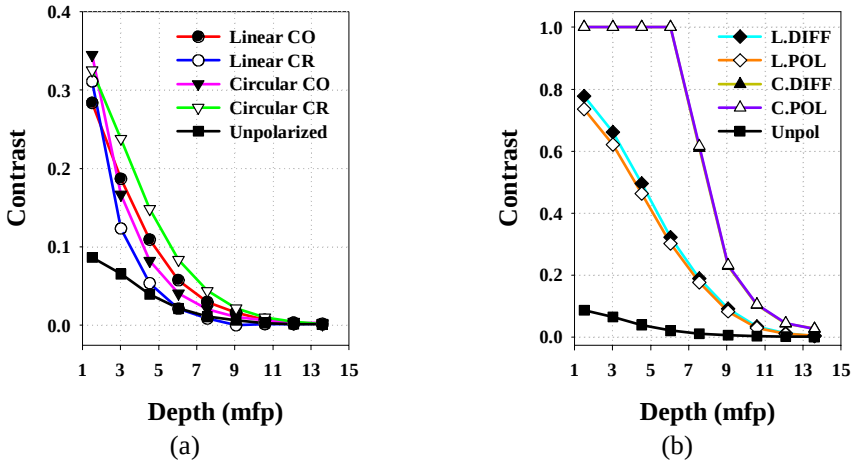

Fig. 3. Contrast plots for a reflecting target under (a) linearly and (b) circularly polarized illumination.

3.2 Scattering target

Figure 4 shows a set of images of an embedded high scattering object (white paint). The phantom had a scattering coefficient of 30cm^{-1}, and absorption coefficient of 0.1cm^{-1}. Despite a higher total illumination, the difference between the CO and CR components was smaller than that of the background for both linear and circular. The result was a dark target in the DIFF image. This smaller difference in a region with greater total illumination led to a dark target with higher contrast in the POL images.

The scattering target was consistently brighter than the background because more light was reflected back from the target than from the background. Both linearly and circularly polarized light were highly scattered from the target so that at 1.5*mfp* the light from target was 52% co-polarized compared to 54% from the background. Because the scattering target and media showed little preference for helicity, the circular and linear images were visually similar.

#6729 - $15.00 US Received 28 February 2005; revised 19 May 2005; accepted 19 May 2005

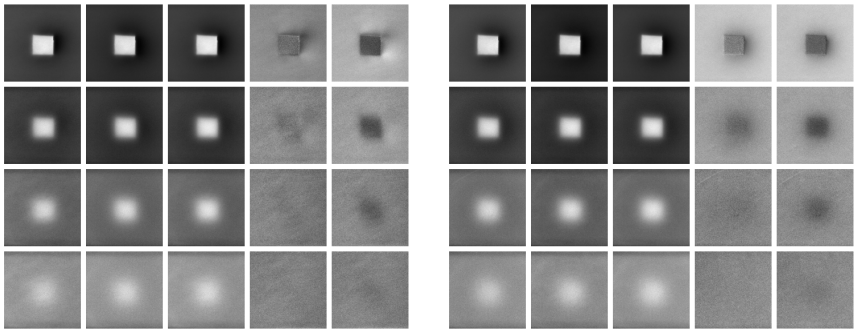

(a) (b)

Fig. 4. Image results of a scattering target acquired with (a) linearly and (b) circularly polarized light. CO, CR, Unpolarized, DIFF, and POL images are listed from left column to right column. Rows correspond to target depth at 1.5, 4.5, 7.5, and 10.5mfp.

Figure 5 shows the calculated image contrast values at different object depths. Linear POL was the best of the linear methods until 6*mfp* where unpolarized light offered equivalent contrast. Among the four components, linear and circular CRs were slightly better than unpolarized light. The circular DIFF image had better contrast than unpolarized light up to 4.5*mfp*. Overall, circular POL offered the best contrast improvement for the scattering target up to 7.5*mfp* depth. The CO and CR components had imaging depths nearly equivalent to the unpolarized light. By contrast the POL and DIFF images were only useful for shallower depths with DIFF being the shallowest. The improved contrast under circular polarization is likely due to the single backscattering or small reflection from the target surface. Reversed helicity from backscattering competed with multiply scattered light from the target and the background, which kept the circular polarization closer to 50% and made the circular POL a better choice.

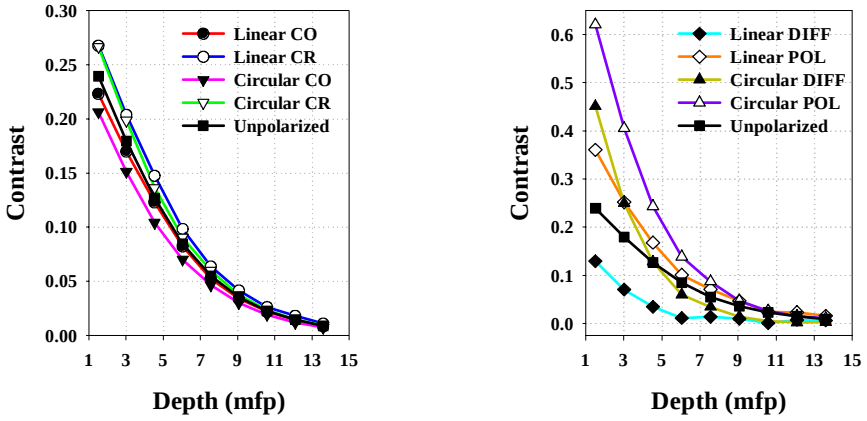

(a) (b)

Fig. 5. Image contrast for a scattering target under (a) linearly and (b) circularly polarized illumination.

3.3 Absorbing target

With absorption we effectively measured the lack of information from the target. The high absorptive target attenuated nearly all of the light that reached it without regard to helicity or orientation so that the target appeared dark in all four components. At 1.5 *mfp* the total amount of light returned from the absorbing target was 18% of that returned from the

#6729 - $15.00 US Received 28 February 2005; revised 19 May 2005; accepted 19 May 2005

background, and only 11% of that returned from a scattering target at the same depth.

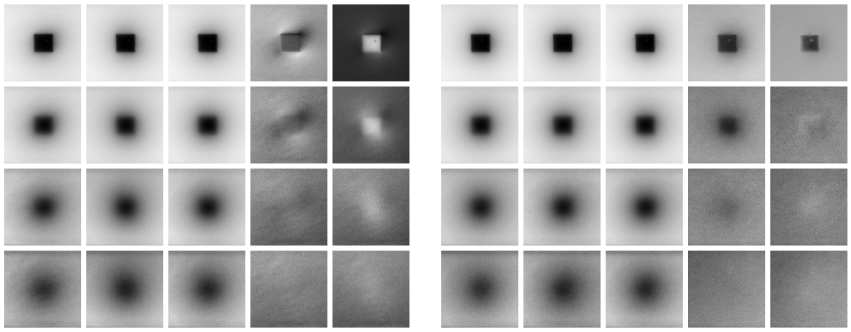

(a) (b)

Fig. 6. Image results of an absorption target acquired with (a) linearly and (b) circularly polarized light. CO, CR, Unpolarized, DIFF, and POL images are listed from left column to right column. Rows correspond to target depth at 1.5, 4.5, 7.5, and 10.5mfp.

Figure 6 shows a set of images of an embedded high absorption object (flat black paint). The background medium had a scattering coefficient of 30 cm^{-1}, and absorption coefficient of 0.1cm^{-1}. Figure 7 shows the calculated image contrast values at different object depths. Unlike the reflecting target, the DIFF and POL did not match. Unlike the scattering target, the linear and circular polarization images were different.

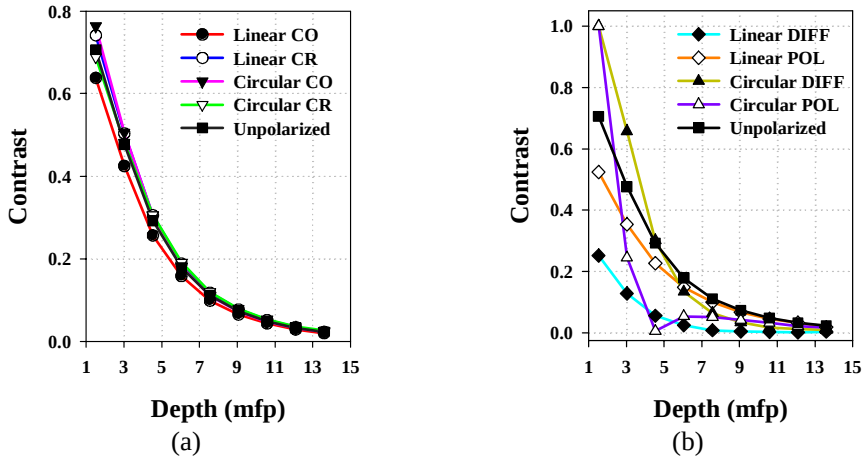

(a) (b)

Fig. 7. Image contrast for an absorption target under (a) linearly and (b) circularly polarized illumination.

The DIFF image presented a dark target because the difference between the linear CO and CR of the target was less than that of the background. The linear POL however presented a bright target, so while there was little light returning from the target region, what light there was maintained the incident polarization. At shallow depths the absorbing target POL gave low value over low value (Eq. (2)) which made it sensitive to relatively small changes in the returning light.

Only the circular DIFF offered slight contrast improvement up to 4*mfp*. This improvement was probably due to residual reflection at the target surface. We can tell this light was reflected off the surface because the circular POL image was the reverse of its linear counterpart at shallow depths. If light were scattered from the absorbing target then it should have lost polarization and appeared identical in linear and circular. Highly scattered background photons competed with the reversed helicity off the surface in circular. The

#6729 - $15.00 US Received 28 February 2005; revised 19 May 2005; accepted 19 May 2005

reversed helicity caused the numerator in POL to be smaller, and this offset the larger denominator in the background areas. A crossover point at 4.5*mfp* in the circular POL contrast was indicative of the two competing sources. At greater depths, light from the surface reflection was quickly washed out by light from the background.

4. Discussion

Absorption, scattering, and reflecting represent the three major contrast mechanisms in optical imaging. The absorption properties are related to sample chemical compositions, such as blood content. The scattering properties are related to sample morphological distributions such as particle size and shapes. Finally, the reflecting can happen at the multilayer boundaries due to refractive index mismatch. The image contrast can originate from all these mechanisms, while different mechanisms have different physiological meanings. Objects with individual optical property were used in this study so that their different behavior can be clarified. By studying how these contrast mechanisms manifest themselves in polarization images, we can gain insight on how to identify different optical targets in acquired images.

4.1 Different target behavior in polarization images

For unpolarized light, different targets may appear similarly. For example, both scattering objects and reflecting objects appeared as bright targets. For a highly scattering phantom (μ_s = 60cm^{-1}, μ_a = 0.1cm^{-1}), the total illumination from the reflecting target was actually less than the background at small depths because of the oblique incidence. Therefore the reflecting object appeared similar to a slightly absorbing target in unpolarized images. On the other hand, in polarization-gated images, the reflecting, scattering and absorbing targets behaved very differently. At shallow depths, the linearly polarized components easily separated the scattering and reflecting targets since the scattering target appeared bright in both CO and CR images, while the reflecting object had different appearance. At deeper depths, the linear POL still revealed a dark scattering target but a bright reflecting target. Similarly, the absorption object and the reflecting object had distinct appearance in polarized images, and the increased POL contrast was an indication of the reflecting target at greater depths.

In our μ_s= 30cm^{-1}, μ_a= 0.1cm^{-1} phantom, the total light (denominator in the POL calculation) from the reflecting target was very close to that from the background. Thus, the resulting POL image had similar contrast as DIFF image. In the phantoms with different μ_s and μ_a, the DIFF and POL contrast were not identical, but still quite close. By comparison, the absorbing and scattering targets displayed markedly different behavior in the DIFF and POL images. For example, POL contrast was higher for the scattering target, while the absorbing target showed a higher contrast in circular DIFF and a lower contrast in linear POL. This suggested that comparing the DIFF and POL values can differentiate the reflecting contrast mechanism from other optical properties.

The scattering and absorbing targets had poorer contrast in the DIFF image than in the components, while the reflecting target was significantly improved. The POL processing improved the image contrast for the predominantly scattering target because highly depolarized light in an area of high illumination gives a small numerator over a large denominator. This situation should be sensitive to the amount of target absorption. As target μ_a increases, the influx of light from the background should make up a larger portion of total light from the target. When the target was predominantly absorptive, the POL contrast was very poor beyond shallow depths. However at these depths, the low denominator in the POL calculation made the contrast very sensitive to small changes in the polarization state of light from the target.

The glossy and flat versions of the scattering and absorbing targets resulted in identical contrast curves although they had distinctly different surface conditions. This observation indicated the surface conditions played insignificant roles comparing to their bulk optical properties. In other words, these differences may have been too insignificant to impact the results in turbid media.

#6729 - $15.00 US Received 28 February 2005; revised 19 May 2005; accepted 19 May 2005

4.2 Effects of background optical properties

After examining the different targets, we next questioned what roles the optical properties of the media would play in the results. The reflective object had displayed the most activity which made it the natural target choice for this experiment. Figure 8 shows the contrast values for POL and unpolarized images acquired with linearly polarized light. The experimental results were obtained from five different phantoms with scattering coefficients ranging from 15cm^{-1} to 60cm^{-1}, and absorption coefficients ranging from 0.05cm^{-1} to 0.2cm^{-1}.

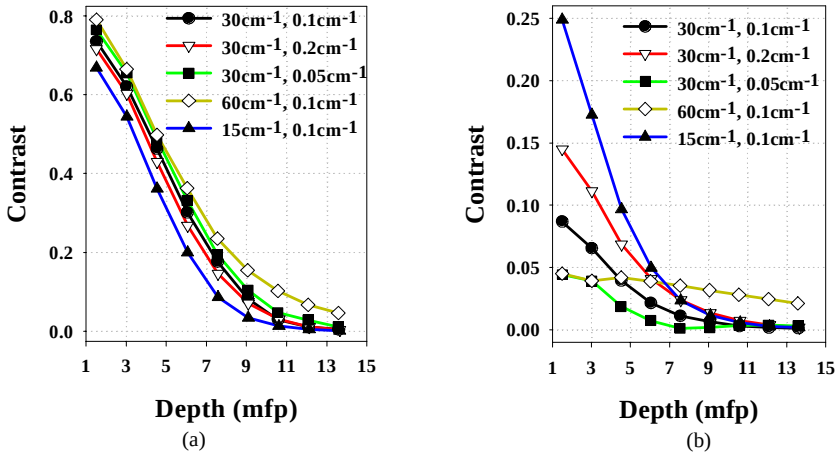

Fig. 8. Contrast of a reflecting target in (a) POL and (b) unpolarized images from phantoms with different scattering and absorption coefficients

Our results indicated that mean-free-path was a good unit for gauging the imaging depth as well as the target size. The POL image indicated the degree of light co-polarization in the target area. As μ_s decreased, the affective area of the target (if represented in *mfp*) also decreased. As such, this "apparent" smaller target blocked less light from the background. Because the background light tended to be unpolarized, the POL contrast became slightly worse. Our experimental results confirmed this behavior; the higher μ_s resulted in better contrast while the lower μ_s led to reduced contrast. As the ratio of μ_s to μ_a decreased, a greater percentage of light was absorbed per *mfp*, which was mainly determined by μ_s. The total illumination from both the background and target area decreased as a result. The impact of this was greater on the target area, as the lower μ_s to μ_a ratio resulted in lower contrast, while the higher μ_s to μ_a ratios resulted in higher contrast.

The contrast curves for the unpolarized light showed a very different response depending on the optical properties of the media (Fig 8b) as did the individual components. The DIFF and POL curves were relatively stable by comparison. The same behavior is seen with circular polarization, albeit with reversed helicity. This suggests that the DIFF and POL contrast measurement might provide a reliable mechanism to detect the same target despite variations in background optical properties.

4.3 Effects of circularly polarized light

Two aspects of circular polarization make it of particular interest. First, under reflection or large angle backscattering, the polarization helicity is reversed. Such change in handedness can differentiate highly reflected and diffused photons and might be useful to improving contrast at tissue boundaries. The second is polarization memory, a tendency for circularly polarized light to maintain its polarization as compared to linearly polarized light. Polarization memory is a function of wavelength and relative size of the scatterers. Small scatterers lead to Rayleigh scattering favoring linearly polarized light, while larger scatterers experience Mie scattering and favor circularly polarized light [12, 15]. It has been

#6729 - $15.00 US Received 28 February 2005; revised 19 May 2005; accepted 19 May 2005

demonstrated [12] that polarization memory might be used to extend the probing depths in polarization imaging.

Polarization memory results in a higher percentage of co-polarized light returning to the surface and a greater depth until polarization is randomized for circularly polarized incident light [15, 16]. However, it was apparently that neither of these conditions was present in our experiments. For five different sample concentrations, the returning background light was consistently near 54% co-polarized for circularly polarized incident light. Memory effects should also present different depolarization curves with depth for linearly and circularly polarized light. However, for the reflective target, aside from reversed helicity, these curves fell off at equivalent rates. Given the high polarization extinction ratio and narrow angle of acceptance in the experiments, we concluded this was not an artifact of the setup, but rather the nature of the phantoms used. Further evidence of this can be seen when examining the contrast curves of the individual targets. While circular polarization provided higher contrast in some situations, it did not significantly improve the maximum imaging depth. A previous study has shown that *Intralipid* can support polarization memory [9] in a transmission configuration. However, it has been shown that the fat emulsion droplets in *Intralipid* vary greatly in size [17] and have average size of <100nm. For a mixture of particles of different sizes, the polarization memory is more influenced by the small size component [18]. As light of 633nm wavelength was used in the experiment, the scattering fell into Rayleigh regime and should have less polarization memory effect.

Despite a lack of polarization memory in the experiments, the reversed helicity from surface reflection provided significant contrast improvement for the reflective target. Our experimental results indicated that circular POL images also gave the best contrast for scattering targets. However, for the absorbing target, circularly polarized light produced images with contrast less than that from linearly polarized light or unpolarized light except for shallow depths, where reversed helicity from small surface reflection improved the circular DIFF contrast.

4.4 Monte-Carlo simulation

Monte-Carlo simulation [13] has been used to examine the impact of target properties. To quantitatively test its numerical accuracy, we compared the behavior for the reflecting target because it has well defined behavior. Figure 9 compares the experimental and simulated POL contrast for linear and circular polarization using $\mu_s = 30\text{cm}^{-1}$, $\mu_a = 0.1\text{cm}^{-1}$ and g = 0.83.

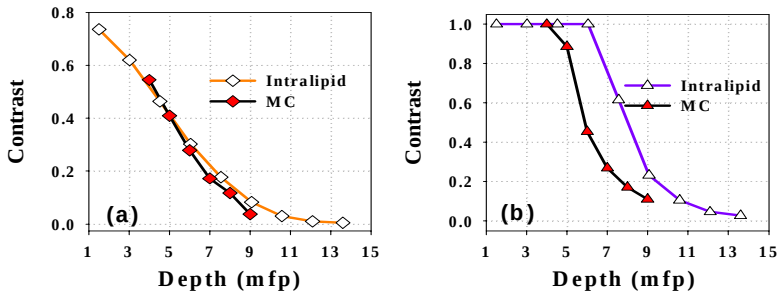

Fig. 9. Monte Carlo simulation of (a) linear and (b) circular POL contrast compared with experimental results.

Under linear polarization, the Monte Carlo results matched very well with the experimental results. For circular polarization the contrast profiles were nearly identical, but simulation results were offset roughly 2.0*mfp* shallower than the experimental results. The Monte Carlo simulation was explicitly coded to simulate Mie scattering. In a departure from the *Intralipid* phantom, the simulations displayed polarization memory resulting in 53.05% linear and 62.12% circular background co-polarization. There are other possibilities that

#6729 - $15.00 US Received 28 February 2005; revised 19 May 2005; accepted 19 May 2005

might have caused this discrepancy. The simulated method of detection may not accurately reproduce the experiments. For example, *Intralipid* has a broad particle size distribution, while single size particle was assumed in Monte Carlo simulation. More experiments using ideal Mie particles (polystyrene spheres) can further clarify these issues. Nevertheless, our results indicated the Monte Carlo simulation can be useful for studying subsurface polarization imaging.

5. Conclusions

Polarization images provided a means to separate the predominantly reflecting, scattering, and absorbing targets where they would otherwise appear similar under unpolarized light. Additionally, no single polarization component or their combinations resulted in significantly improved contrast for all of the targets. For the reflecting target the gated polarization images (i.e., the POL and DIFF images) offered imaging depth slightly better than the best raw component image. For scattering target, the components images had slightly larger imaging depth. For absorbing target, the gated polarization images were significantly worse than the raw component images. Results from the reflective target showed the POL and DIFF contrast are relatively stable with respect to the optical properties of the background media.

The Monte-Carlo simulation proved useful in exploring target and media combinations prior to complicated laboratory arrangements. Experimental results confirmed the simulation predictions for the contrast improvement from the three predominant targets. For linear polarization the simulation results were a strong numerical match for the experimental results from the reflecting target. The circular behavior showed small discrepancies between simulation and experimental results and need further studies.

In this examination off-normal incidence with normal detection was used to avoid specular reflection from the phantom surface. However, our results on different targets' behavior in scattering media should be applicable to coaxial measurement configuration. While targets with pure optical properties were used in this study, many different properties may appear in a single target in practice. The final contrast would be a weighted summation of these different contributions and our results may help to identify the dominant contrast mechanisms. Although *Intralipid* phantoms have been widely used, many biological tissues may display additional polarization properties [9], especially when there are strongly organized structures [7, 8]. More studies are necessary to clarify these issues.

Acknowledgments

This research was made possible by a research board grant from the University of Missouri. We would like to thank Mr. Jinjun Xia for measuring sample optical properties.

#6729 - $15.00 US Received 28 February 2005; revised 19 May 2005; accepted 19 May 2005